Realization & HIL Testing of Wind Turbine Emulator Based on DTC Squirrel Cage Induction Motor Drive

[1]Osama M. ARAFA
Oarafa2004@yahoo.com,+201065549830

[2] M. E. ABDALLAH
eng.msa12@yahoo.com,+201151141130

[3]Ghada A. ABDEL AZIZ
ghada_ahmed@eri.sci.eg, +201095311099

[1,2,3]Power Electronics and Energy Conversion Department, Electronics Research Institute, Cairo, Egypt

Abstract— *Direct torque control (DTC) is known to produce the fastest torque response in AC drives. In this paper, a wind turbine emulation (WTE) system using a squirrel cage induction motor (SCIM) working in a DTC mode is designed, implemented, and tested experimentally using Hardware-in-loop (HIL). The flux estimation is based on the current model where two stator currents and the rotor speed are measured. The DTC is realized using a space vector modulator to avoid variable switching frequency associated with the DTC switching tables. dSPACE Microlabox is used to handle the real-time control programmed in SIMULINK. Typhoon HIL402 is used to emulate the inverter, the machine, the connected mechanical load, and the feedback sensors of the current dc link voltage and speed. Thanks to the great flexibility offered by the HIL technique, a variety of tests has been conducted to validate the overall system performance. The tests include step change of load, step change of wind speed, operation under stochastic wind speed variation and torque-speed characteristics' of the emulated wind turbine at different feeds of wind speeds and coupled mechanical loads. Testing results verified the perfect fit of DTC in WTE application and the effectiveness of the HIL testing technique.*

Key words*: Direct torque control (DTC), squirrel cage induction motor (SCIM), wind energy conversion systems (WECS), wind turbine emulator (WTE), current-model based flux estimator, Hardware-in-Loop (HIL).*

NOMENCLATURE

$V_{s\alpha}$, $V_{s\beta}$, $I_{s\alpha}$, $I_{s\beta}$	Stator voltages/currents in $\alpha\beta$-frame
$I_{r\alpha}$, $I_{r\beta}$	The rotor currents in $\alpha\beta$-frame
$\Psi_{s\alpha}$, $\Psi_{s\beta}$	The stator flux linkages in $\alpha\beta$-frame
$\Psi_{r\alpha}$, $\Psi_{r\beta}$	The rotor flux linkages in $\alpha\beta$-frame
Ψ_s, Ψ_r	The stator and rotor flux linkages
$\Psi^*_{r\ nom}$	The nominal flux linkage of the rotor
R_s, L_s	The stator resistance and inductance
R_r, L_r	The rotor resistance and inductance
σ	The total leakage coefficient
L_m	The magnetizing inductance
p	Number of pair poles
J	Inertia of the rotor and connected load
B	Friction coefficient
T_L	Load torque
V_{dc}	The DC-link voltage
ρ	The air density
R	The radius of the rotor's swept area
v_w	The wind speed
P_m	The nominal power of the SCIM
P_t	The nominal turbine power
Ω_m	The rotor angular speed
Ω^*_m	The reference rotor angular speed

1. INTRODUCTION

Many systems have been designed for the purpose of wind turbine emulation (WTE) [1]-[3]. The emulator is coupled to an electrical generator to compose a complete wind energy conversion system (WECS) as the emulator generates electromagnetic torque similar to the aerodynamic torque at any given wind speed and shaft rotational speed. Emulators provide more control and flexibility due to the fact that selectable wind profiles, rotational speeds, and repeatable testing conditions can be provided easily in the laboratory.

Different motor types have been used to realize emulators [4], [5]. In particular, DC machines were used for emulating wind turbine [6]-[9] due its simple control and rapid torque response that can be realized in a wide rotational speed range. However, DC motors are bulky, expensive, and continuous maintenance is required due to the existence of commutators and brushes. Therefore, emulators using permanent magnet synchronous motors (PMSMs) [10], [11] are excellent alternatives to DC-based ones as they are free from brushes. By using field orientation control (FOC), PMSMs can offer a

torque response and a wide speed range comparable to those of the DC machine.

Owing to the modern achievements in digital signal processing and subsequent high-quality control of AC machines, emulator based on squirrel cage induction motors (SCIMs) which are more

frame (α-β) fixed with the stator. The control strategy comprises cascaded loops in which outer torque and flux loops produce reference currents for the inner control loops of stator currents, a concept that is quite different from DTC. Cascaded loops,

torque response than DTC; as it involves current control loops as well.

Direct torque control (DTC) abandons the stator current control philosophy which is a characteristic of FOC and heads to flux and torque control by directly modifying the stator voltage in accordance with the torque and flux errors. The control of stator voltages is done such that the stator flux performs two essential tasks. The first task is to maintain the rotor flux at the desired magnitude (rotor flux is considered entirely aligned to the direct axis of the synchronously rotating frame of reference). The second task is to adjust the angle between the stator flux and the rotor flux large properly to develop the desired torque. Thus, it offers a good tracking performance for both electromagnetic torque and flux magnitude [15].

DTC is characterized by the fast dynamic response, the structural simplicity, and the robustness against parameter uncertainties. Also, it is one of the most powerful techniques used recently to control the SCIM. The DTC was originally implemented by using switching tables and it was initially called direct self-control scheme [16]-[18]. It was also called independent hysteresis control in flux and torque [19]-[24]. In its original implementation, DTC was characterized by the absence of PI regulators, the absence of coordinate transformations, and the absence of current regulators, and PWM signals generators. Therefore, DTC offers simplicity, good performance, and robustness [25]. However, hysteresis controllers result in variable switching frequency which increases with narrowing the hysteresis band and it needs short control period of about 25 μs to achieve acceptable performance [26], [27]. Indeed, the torque and the flux vector calculated from stator parameters and measured stator quantities only suffer from inaccuracy with respect to the real flux vector. Thus, it would lead to incorrect control and undesirable torque and current ripples, and it cannot robust became more cost-effective as well than PMSM-based ones [12]. In [13], the emulator is based on an SCIM with torque and flux control. The torque and flux are controlled with closed-loop stator current in the two-phase reference

however, offer slower dynamic torque response. In [14], emulation is done using an SCIM and FOC to obtain a fast torque control of the motor that could match the fast torque dynamics of a real wind turbine. It is generally agreed that FOC has slower guarantee stability especially at low speeds. Thus, correction methods based on including terms belonging to rotor quantities and parameters were applied as in [26]-[29] to improve the overall performance of the DTC. Another correction method in [30] suggests using appropriate component of stator current vector to correct flux estimation.

In this paper, a modified torque control method known as DTC-SVM is used. The DTC-SVM uses two measured stator currents, measured DC-link voltage, and measured rotor speed. A space vector modulator (SVM) is used to control the power switches of the inverter at a predetermined fixed frequency. The model used for flux estimation is traditionally known as current-model. This method provides excellent overall performance and removes a lot of disadvantages associated with the classical DTC including the variable switching frequency. The proposed method also reduces the torque, flux, and current ripples while preserving the merit of fast DTC torque response. The selected implementation is an optimum choice for this application since speed measurement is essential for WTE and hence the readily available measurements are used.

The paper explains in sufficient details the different aspects of the implementation and it is organized as follows: the wind turbine mathematical model is presented in section 2. The mathematical model of the SCIM, the flux linkage and torque estimators are presented in section 3. Section 4 presents the whole DTC-SVM control scheme and the design of the flux and torque PI controllers. The experimental setup, and the results are presented and discussed in section 5. Section 6 has the conclusion of the paper.

2. WIND TURBINE MODEL

The mechanical output power of the wind turbine [31] is given in (1):

$$P_m = \frac{1}{2}\rho\pi R^2 C_p(\lambda,\beta)v_w^3 \quad (1)$$

The power coefficient is defined as the ratio of the turbine mechanical power to the power available by the wind. This coefficient is a function of tip speed ratio and the pitch angle of the blades in degree. TSR is the ratio of the blade linear tip speed to the wind speed as illustrated in (2):

$$\lambda = \frac{\Omega_m R}{v_w} \tag{2}$$

The aerodynamic mechanical torque of the wind turbine is given by:

$$T_m = \frac{1}{2}\frac{\rho\pi R^3 C_p(\lambda,\beta)v_w^2}{\lambda} \tag{3}$$

As mentioned in [32], the power coefficient, $C_p(\lambda,\beta)$, is a nonlinear function of the tip speed ratio, λ, and the blade pitch angle, β. The $C_p(\lambda, \beta)$ curve is unique characteristics of wind turbine design and it is identified from field tests of the turbine. An empirical equation is normally used to model the $C_p, \lambda,$ and β surface based on the turbine characteristics, as illustrated in (4) [9], [33]:

$$C_p(\lambda,\beta) = C_1.\left(C_2.\frac{1}{\lambda_i} - C_3.\beta - C_4\right)e^{\frac{C_5}{\lambda_i}} + C_6.\lambda \tag{4}$$

where C_1 to C_6 are constants and λ_i is given in (5):

$$\frac{1}{\lambda_i} = \frac{1}{\lambda + 0.08\beta} - \frac{0.035}{\beta^3 + 1} \tag{5}$$

Table 1 indicates the values of the parameters C_1 to C_6 for a specific turbine design [8]. For the set of parameters of Table 1, Fig. 1 shows the power curve at $\beta = 0$ deg.

TABLE 1
THE POWER COEFFICIENT EQUATION PARAMETERS

C_1	C_2	C_3	C_4	C_5	C_6
0.5176	116	0.4	5	21	0.0068

The maximum theoretical value of the power coefficient ($C_p = 0.48$) is achieved at $\lambda = 8.108$ for zero pitch angle.

From the wind turbine power and torque in (1) and (3), it can be noticed that the emulator inputs are the wind speed, the blades pitch angle, and the rotor speed and the output is the torque which is produced by the real turbine for this given set of inputs.

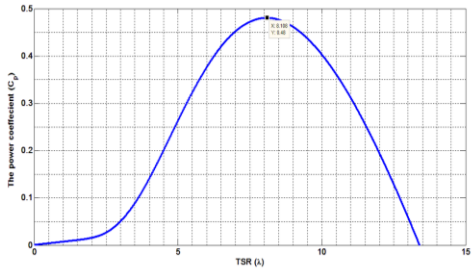

Fig. 1. Typical power coefficient curve at $\beta = 0$

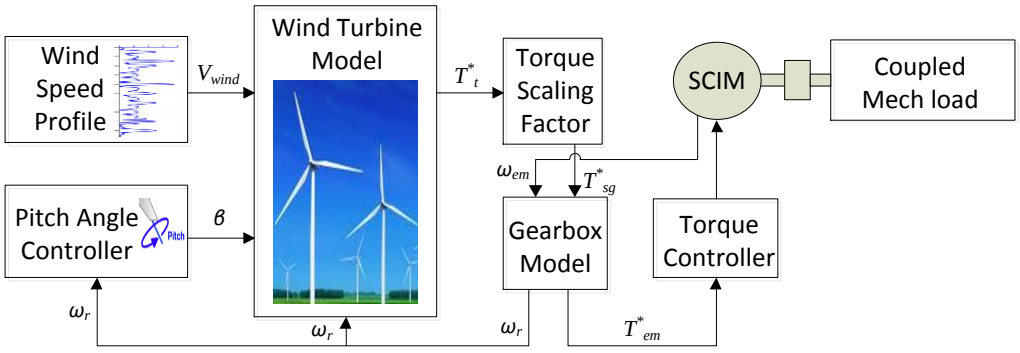

Fig. 2. Complete strategy of emulating wind turbine

Fig. 2 illustrates schematically the control flow within the emulator system. The wind speed profile is supplied using recorded measurements from an actual site or can be generated artificially using a proper algorithm [14]. In real WECS, the blades pitch angle is controlled by a dedicated subsystem to limit the power converted so that it does not exceed the power rating of the whole drive train and to bring the WECS to a complete stop in case of emergency or very strong wind gust. The wind turbine model block is based on (1)-(5) and it is responsible for calculating the torque that is generated by the turbine for each set of input values (V_{wind} in m/s, β in deg. and ω_r in rad/s).

The torque generated by the turbine T_t^* is scaled down by the factor S_t to T^*_{sg} to enable simulating a large turbine using a smaller motor rating without damage.

$$S_t = \frac{P_m}{P_t} \quad (6)$$

The low-speed side torque T^*_{sg} is further scaled down with the inverse ratio of the gearbox to get the torque of the high-speed side T^*_{em} that is generated by the SCIM. The SCIM control is responsible for the instantaneous realization of the torque T^*_{em}. The rotational speed of the low-speed side of the gearbox ω_r is fed back to the wind turbine block to complete the data required for calculating the turbine torque.

3. SCIM Mathematical Model and Flux Estimator Model

The voltage equations of the SCIM in the stator stationary frame ($\alpha\beta$-frame) are given in (7)-(10) [34]:

$$V_{s\alpha} = R_s I_{s\alpha} + \frac{d\psi_{s\alpha}}{dt} \quad (7)$$

$$V_{s\beta} = R_s I_{s\beta} + \frac{d\psi_{s\beta}}{dt} \quad (8)$$

$$0 = R_r I_{r\alpha} + \frac{d\psi_{r\alpha}}{dt} + p\Omega_m \psi_{r\beta} \quad (9)$$

$$0 = R_r I_{r\beta} + \frac{d\psi_{r\beta}}{dt} - p\Omega_m \psi_{r\alpha} \quad (10)$$

The flux linkage equations are given in (11)-(17):

$$\psi_{s\alpha} = L_s I_{s\alpha} + L_m I_{r\alpha} \quad (11)$$

$$\psi_{s\beta} = L_s I_{s\beta} + L_m I_{r\beta} \quad (12)$$

$$|\psi_s| = \sqrt{\psi_{s\alpha}^2 + \psi_{s\beta}^2} \quad (13)$$

$$\theta_{\psi s} = atan2(\psi_{s\beta}, \psi_{s\alpha}) \quad (14)$$

$$\psi_{r\alpha} = L_r I_{r\alpha} + L_m I_{s\alpha} \quad (15)$$

$$\psi_{r\beta} = L_r I_{r\beta} + L_m I_{s\beta} \quad (16)$$

$$|\psi_r| = \sqrt{\psi_{r\alpha}^2 + \psi_{r\beta}^2} \quad (17)$$

The electromagnetic torque T_{em} is given by:

$$T_{em} = \frac{3p}{2}\left(\psi_{s\alpha} I_{s\beta} - \psi_{s\beta} I_{s\alpha}\right) \quad (18)$$

The motion equation is expressed as:

$$\frac{d\Omega_m}{dt} = \frac{1}{J}[T_{em} - T_L - B\Omega_m] \quad (19)$$

The previous set of equations involving fluxes and currents can be rearranged to use the stator currents and the rotor speed ($I_{s\alpha}$, $I_{s\beta}$, Ω_m) as known inputs and the fluxes ($\psi_{s\alpha}, \psi_{s\beta}, \psi_{r\alpha}, \psi_{r\beta}$) as outputs as illustrated in (20)-(25).

$$\psi_{s\alpha} = \sigma L_s [I_{s\alpha} + \frac{L_m}{\sigma L_s L_r} \psi_{r\alpha}] \quad (20)$$

$$\psi_{s\beta} = \sigma L_r [I_{s\beta} + \frac{L_m}{\sigma L_s L_r} \psi_{r\beta}] \quad (21)$$

$$\frac{d\psi_{r\alpha}}{dt} = -R_r I_{r\alpha} - p\Omega_m \psi_{r\beta} \quad (22)$$

$$\frac{d\psi_{r\beta}}{dt} = -R_r I_{r\beta} + p\Omega_m \psi_{r\alpha} \quad (23)$$

$$I_{r\alpha} = \frac{1}{\sigma L_r}\psi_{r\alpha} - \frac{L_m}{\sigma L_s L_r}\psi_{s\alpha} \quad (24)$$

$$I_{r\beta} = \frac{1}{\sigma L_r}\psi_{r\beta} - \frac{L_m}{\sigma L_s L_r}\psi_{s\beta} \quad (25)$$

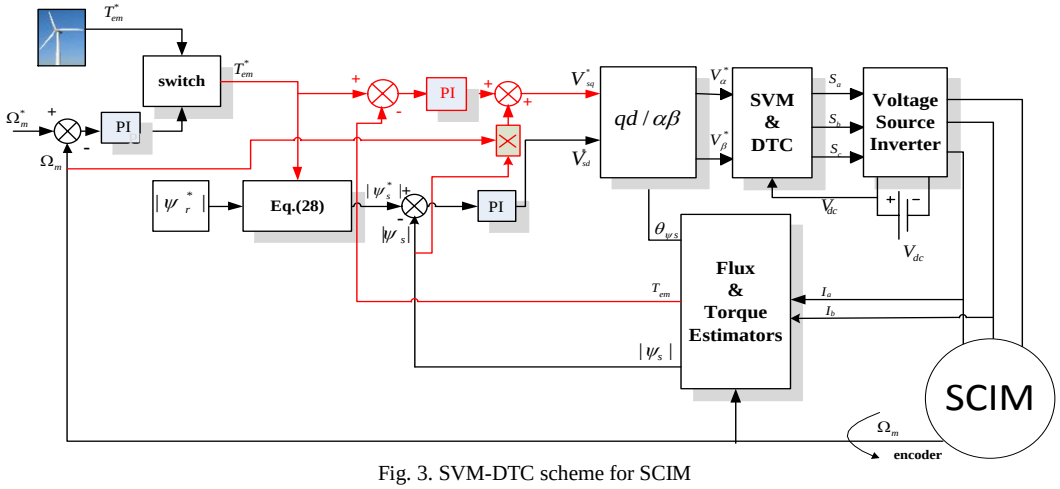

Fig. 3. SVM-DTC scheme for SCIM

Equations (20) to (25) constitute the mathematical basis of the flux estimator. These equations in their presented form involve algebraic loops. Therefore, it is necessary to adopt a recursive solution by

inserting one sample time lag after the integrators which provide the values of $\psi_{r\alpha}$ and $\psi_{r\beta}$.

4. The DTC-SVM control of the SCIM

The core concept of the DTC is that the stator flux response is too fast compared to the rotor flux response. At any rotational speed, the stator flux magnitude and its angle with respect to the rotor flux can be controlled by applying appropriate stator voltages. In the asynchronously rotating frame of reference (*dq*-frame), the rotor flux can be considered entirely existing in the *d*-axis. The fast response of the stator flux enables controlling its *d*-axis and the *q*-axis components appropriately such that the rotor flux magnitude is kept constant and the torque angle is changing according to the desired torque.

In Fig.3, the whole DTC-SWM scheme is depicted. The measured stator currents (two currents are sufficient since the sum of the three currents is zero) are converted to the stationary *αβ*-frame. The measured rotor speed and the *αβ*-currents are fed to the flux estimation block based on (20)-(25). The torque is estimated using (18). The error between the stator flux reference and the estimated stator flux is used to drive the flux PI controller which computes the reference *d*-axis voltage of the stator. The error between the torque reference and the estimated torque (red colored lines) is used to drive the torque PI controller which computes the reference *q*-axis voltage of the stator. The angle used to transform from the *dq*-frame to the *αβ*-frame is the stator flux angle $\theta_{\psi s}$ given by (14). The resulting reference *αβ*-voltages from the inverse Park transform are used to drive the Space Vector Modulator which receives the DC voltage as a measurement and the switching period as a parameter [35]. To improve the dynamic response of the emulator, decoupled control of flux and torque should be ensured. This requires maintaining the rotor flux constant irrespective of the torque generated by the machine. From the *dq*-model of the SCIM when $\psi_{rq} = 0$, the stator flux linkages in *dq*-frame ψ_{sd}, ψ_{sq} can be obtained from (26) and (27) [34]:

$$\psi_{sd} = \frac{L_s}{L_m}(\psi_r + \frac{L_r}{R_r}\sigma\,\frac{d\psi_r}{dt}) \tag{26}$$

$$\psi_{sq} = \frac{2}{3p}\frac{L_r}{L_m}\sigma L_s\,\frac{T_{em}}{\psi_r} \tag{27}$$

To maintain $\frac{d\psi_r}{dt} = 0$ (i.e. maintaining constant rotor flux), it is therefore required to set the reference stator flux magnitude according to (26) and (27) as in (28):

$$|\psi_s|^* = \sqrt{{\psi_{sd}}^{*2} + {\psi_{sq}}^{*2}} = \sqrt{\left(\frac{L_s}{L_m}{\psi_r}^*\right)^2 + (\frac{2}{3p}\frac{L_r}{L_m}\sigma L_s\,\frac{{T_{em}}^*}{{\psi_r}^*})^2} \tag{28}$$

The product of the electrical rotor speed and the estimated stator flux magnitude ($p\Omega_m * |\psi_s|$) known as the rotational voltage is fed forward and summed with the *q*-axis voltage resulting from the PI of the torque controller to enhance the dynamic response of the torque controller over the whole speed range.

The emulator shown in Fig.3 is also equipped with a classical proportional-integral (PI) speed regulator to initialize the drive train to a known initial speed from a standstill. Then it leaves the speed control mode and starts tracking the reference torque commanded by the wind turbine block. In torque tracking mode, the shaft speed is left float and changes in response to the dynamic balance between the wind turbine torque developed by the SCIM and the coupled generator (i.e. load) torque. Ahead of activating the torque tracking mode, the integrator of the speed PI regulator is reset and during torque mode, the speed PI regulator is fed with zero speed error. Speed regulator comes back into control in case of emergency (e.g. sudden loss of load which is identified via over speed beyond a certain limit) or in case of intentional switching by the operator.

The design of the flux and torque controllers is based on the assumption that the used scheme sufficiently decouple the torque and flux loops due to holding the rotor flux constant. In the following section, the design of the PI controllers of the flux and torque loops will be presented. Also, the PI used for speed regulation in the speed control intervals will be also presented.

A. The Stator Flux Controller Design

The flux control loop is shown in Fig. 4. If the small resistive voltage drop is neglected, the transfer function between the *d*-axis voltage and the flux magnitude is simply an integrator as illustrated in (29). The inverter transfer function can be approximated as in (30):

$$\frac{\psi_s}{V_d} = \frac{1}{S} \tag{29}$$

$$\frac{V_d}{V_d^*} = \frac{e^{-ST_d}}{(1+ST_s)} \quad (30)$$

where T_d is the time delay inserted to avoid shoot through in inverter legs and T_s is the sampling period for the discrete controller.

According to the symmetry criterion for controller design [34], and provided that T_d is too small compared to T_s (in this paper: 2 and 50 µs, respectively), the PI used for flux control might have the following proportional and integral gains in (31) and (32):

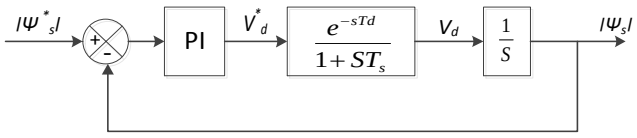

Fig.4. Flux control loop

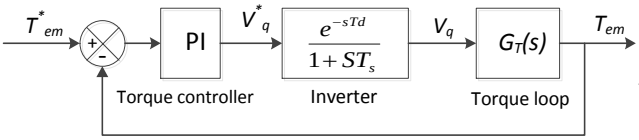

Fig.5. Torque control loop

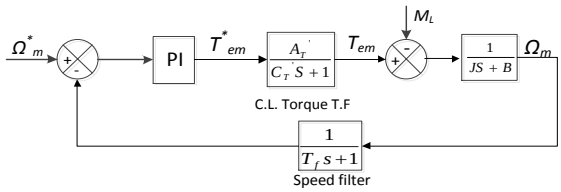

Fig.6. Speed control loop

$$K_{p\psi} = \frac{1}{2T_s} \quad (31)$$

$$K_{i\psi} = 4\,T_s \quad (32)$$

It should be mentioned that the smaller T_s, the closer the system to quasi-continuous assumption and hence, the better controller performance is obtained.

B. The Torque Controller Design

A second order open loop transfer function between the torque and the *q*-axis voltage can be expressed as follows [34]:

$$G_T(s) = \frac{T_{em}}{V_q} = \frac{A_T S}{S^2 + B_T S + C_T} \quad (33)$$

where $A_T = \frac{3p\psi_s}{2\sigma L_s}$, $B_T = \frac{R_s L_r + R_r L_s}{\sigma L_s L_r}$, $C_T = \frac{3p^2{\psi_s}^2}{2\sigma L_s J}$

The torque control loop is depicted in Fig.5. The root locus method can be used to design the controller parameters. The single input single output (SISO) control design tool in MATLAB has been used to design the torque PI parameters ($K_{pT} = 40, K_{iT} = 140$).

C. The Speed Controller Design

The speed control loop is depicted in Fig.6, The closed-loop transfer function of the torque control loop is approximated to a first-order system as in (34) [34].

$$G_T'(s) = \frac{A_T'}{C_T'S + 1} \quad (34)$$

where $A_T' = \frac{A_T K_{pT}}{C_T K_{iT} + A_T K_{pT}}$, $C_T' = \frac{A_T B_T K_{pT} K_{iT}}{C_T K_{iT} + A_T K_{pT}}$

A low-pass filter (LPF) whose transfer function is shown in Fig.6 is normally inserted in the speed feedback path. The whole plant transfer function can be approximated to:

$$G(s) = \frac{A_T' e^{-ST_d}}{JS(T_a S + 1)} \quad (35)$$

where T_a is the sum of all time constants including the speed low-pass filter T_f. The symmetry criterion can be used for the design of the speed controller parameter and the controller parameters are given in (36) and (37):

$$K_{ps} = \frac{J}{2T_a} \quad (36)$$

$$K_{is} = 4\,T_a \quad (37)$$

5. Performance Investigation

The experimental setup shown in Fig.7.a is used to validate the designed control and to verify the system overall performance.

The setup is based on Hardware-in-Loop (HIL) emulation of the DC source, DC-link, inverter, the SCIM (appendix I) and the coupled mechanical load. The HIL used is HIL402 from Typhoon HIL. The DTC control strategy is executed by dSPACE Microlabox DSP. The allocation of the system components to the hardware resources is depicted in Fig.7.b. Two different colors are used to distinguish the two main resources (HIL-402 and Microlabox). The analog signals exchanged between the two subsystems are the two currents measurement, the DC-link voltage measurement, and the coupled

mechanical load measurement. The digital signals sent from the Microlabox controller to the HIL402 are the three inverter switching signals and the switching signal for the chopper used for regulating the DC-link voltage (the latter is not shown in Fig.7.b). PWM signals complementing and dead time insertion are handled internally by the HIL-402. The digital signals sent from the HIL402 to the Microlabox include the encoder channels A and B.
Both platforms have their own visualization interface. The dSPACE has the Control Desk software which allows monitoring the system states and allows also changing the gains of the PI controllers online during runtime. The HIL402 also has HIL SCADA which allows similar functionality.

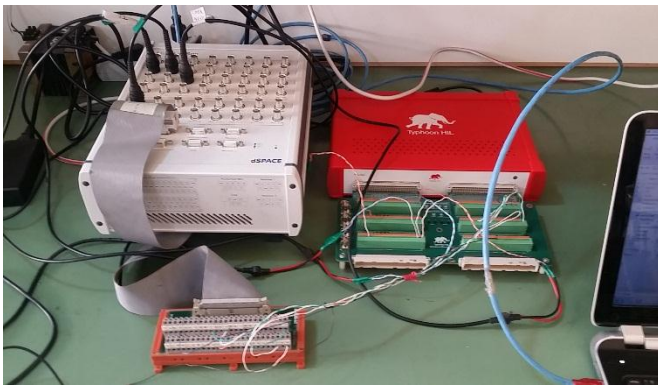

a. The dSPACE Microlabox & Typhoon HIL402

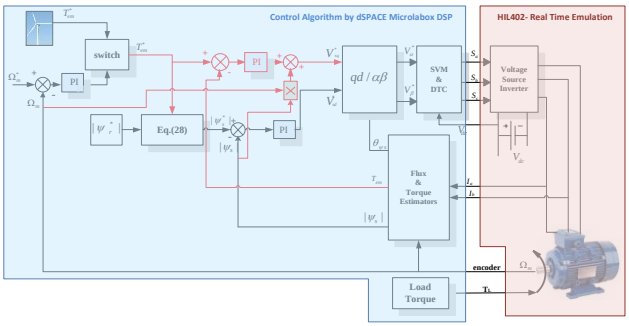

b. Allocation of system components to H/W resources
Fig.7. Experimental Setup

The emulated machine is fitted with an incremental encoder with 6000 pulses per turn for measuring the speed. A two-level three-phase IGBT inverter running at 20 KHz with 2 µs dead time is used to control the SCIM voltages. The control program cycle time is 50 µs. The captures taken from dSPACE Control Desk are exported to MAT files and plotted using MATLAB.

A. Torque-Speed Characteristics of WTE at Different Wind Speeds

he first test of the WTE considers the validation of the torque-speed characteristics at different feeds of wind speed as shown in Fig. 8. This test is done by selecting a fixed wind speed for each curve, then the coupled load is slightly increased from no-load or partial load to breaking load in a relatively short interval.

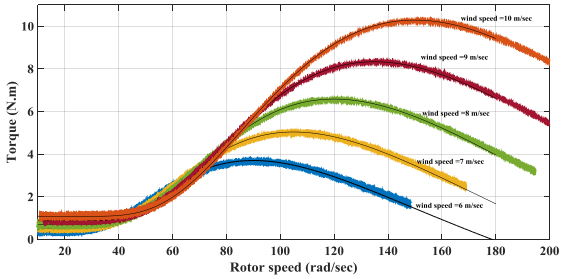

Fig.8. Torque-speed characteristics of the emulator versus the wind turbine

The pairs of the rotational speed and the developed torque are recorded from the maximum speed (right-hand side of the figure) to the zero speed (left-hand side of the curve). The test is repeated for arbitrary wind speeds, e.g. 6, 7, 8, 9, and 10 m/s so that the family of curves presented in Fig.8 is obtained. The smooth black curves are the theoretical ones maenwhile, the coloured are the actual ones. From Fig.8, it is evident that the system perfectly emulates the theoretical torque-speed characteristics of the wind turbine.

B. WTE Performance under Sudden Load Change and Sudden Wind Speed Change

Fig. 9 depicts the dynamics of the WTE under a sudden change of load and a sudden change in wind speed. There are two speed-torque characteristics lines shown for the load, the red one represents the load line (including the frictional torque) that results in maximum power at all wind speeds, the purple one is only half of the red line.

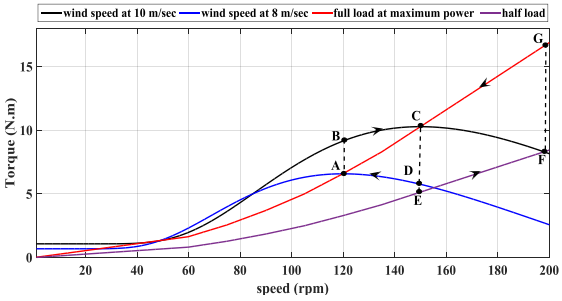

Fig. 9. Torque-speed characteristics of turbine and load under load step change and wind speed step change tests

There are two torque-speed characteristic curves shown for the turbine, the black one corresponds to 10 m/s wind speed and the blue one corresponds to 8 m/s wind speed. In the sudden change of load while the wind speed is at 10 m/s, If the load line is suddenly changed from the purple to the red, the load torque will jump from the initial equilibrium point F to *G* then moves along the red curve to *C* accompanied by a deceleration in the rotor speed. The torque provided by the turbine increases by moving along the black curve from *F* to *C*. At the end of this transient period, the operation will settle at the new equilibrium point *C*. The cycle is reversed if the load line is suddenly switched from the red to the purple, and hence, the operation moves from *C* to *F* again passing through the point *E* instead of *G* and accompanied by an acceleration of the rotor speed.

C. WTE Performance under Sudden Load Change

These dynamics of the WTE under sudden load change are shown in Fig.10. The difference between motor torque and load torque is merely the frictional torque.

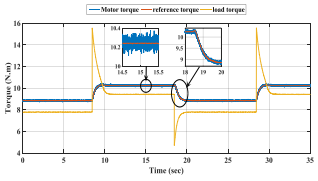

a. Motor torque, reference torque load torque

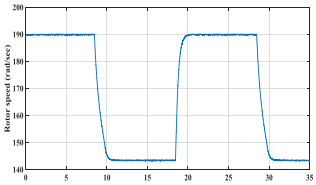

b. Rotor Speed

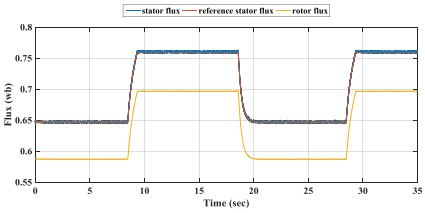

c. Reference stator flux, actual stator flux, and rotor flux

Fig.10. The dynamics of WTE under sudden load change.

It is evident that the motor torque perfectly follows the reference as in Fig. 10.a. Fig.10.b depicts the transient deceleration and acceleration in rotor speed. Fig.10.c depicts the flux weakening operation of the machine which allows overspeed operation with reduced torque capability for successful WTE.

D. WTE Performance under Sudden Change in Wind Speed

The sudden change in wind speed is tested by switching the wind speed feed to the turbine block between 8 m/s and 10 m/s as shown in Fig.11.a while the load is set to the MPPT load line.

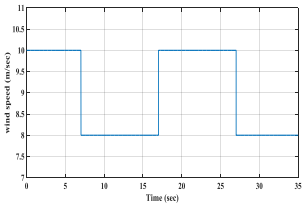

a. Wind speed profile

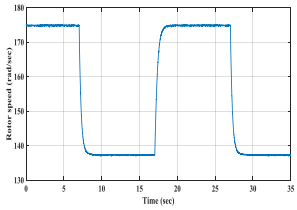

b. Rotor speed profile

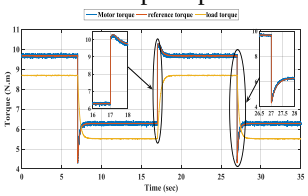

c. Reference torque, motor torque and load torque

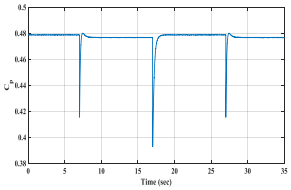

d. Coefficient of power conversion (C_p)

Fig. 11. The dynamics of WTE under sudden change in wind speed

Referring to Fig.9, the sudden change from wind speed from 8 m/s to 10 m/s is represented by the jump from point *A* to point *B* as the turbine developed torque is higher than the coupled load torque as illustrated in Fig.11.c, therefore acceleration in rotor speed continues until the new equilibrium point *C* is reached. The difference between turbine developed torque and load torque is due to frictional torque. The reversed cycle exists when the wind speed is changed from 10 m/s to 8 m/s. The turbine operating point jumps from point *C* to point *D* at which the torque delivered by the turbine is less than the torque applied by the load as shown in Fig.11.c and hence, deceleration commences and continues until the equilibrium point *A* is reached. Fig.11.b shows theacceleration/deceleration transient intervals in rotor speed as well as the rotor speed at equilibrium operation points *A* and *C*. Since the applied load is set to the MPPT line, the coefficient of power conversion is close to the theoretical maximum value 0.48 as depicted in Fig.11.d except for the short transient intervals upon sudden change of wind speed.

E. WTE Performance under Stochastic Wind Speed

The goal of this test is to study the system performance under stochastic wind speed profile. A realistic wind model is essential for a full assessment of the emulator performance. The details of implementation of a realistic wind speed can be

found in [36-39]. Fig.15.a represents the stochastic wind speed profile used in this test

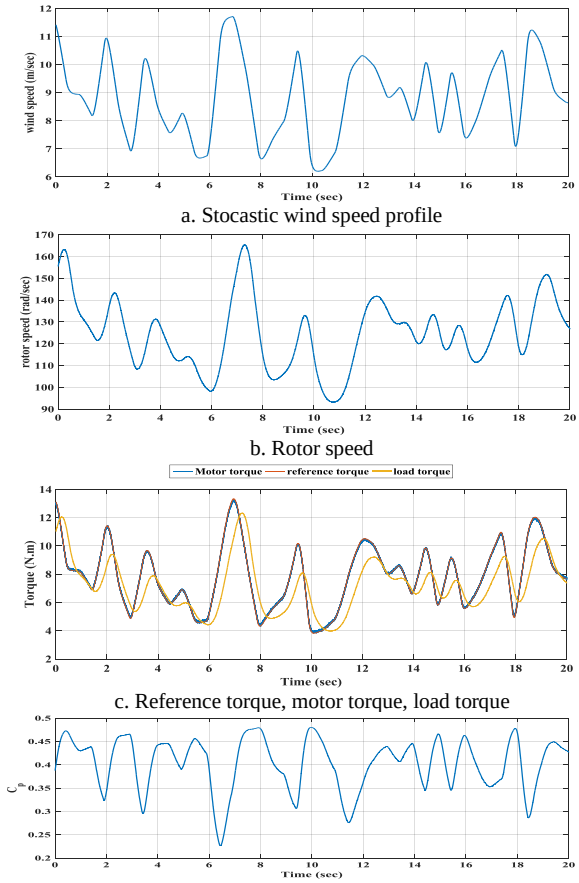

a. Stocastic wind speed profile

b. Rotor speed

c. Reference torque, motor torque, load torque

d. Power conversion coefficient (C_p)

Fig. 15. WTE performance under stochastic change of wind speed

The coupled load follows the MPPT load curve. Fig.15.b depicts the resulting rotor speed profile and Fig.15.c depicts the reference torque, the motor developed torque, and the load torque. Although the coupled load follows the MPPT curve, Fig.15.d indicates that the power conversion coefficient is not maintained at the maximum value of 0.48. The reason is that the MPPT strategy needs to dynamically adjust the load torque rather than fixing it all the time such that the rotor speed always follows the optimum tip speed ratio. Only in the active MPPT mode, C_p can be dynamically held at the maximum value. However, the application of MPPT is not included in this test.

6. CONCLUSION

A wind turbine emulator (WTE) has been implemented using an SCIM to reproduce the characteristics of a real wind turbine in the laboratory. A lot of tests have been done on the implemented system to check its dynamic performance. All tests have been implemented using Hardware-in-loop system which gives a great flexibility in the test scenario design at a very affordable cost.

The DTC control of the SCIM allows the motor to successfully track the reference torque generated by the turbine emulation block under a variety of sever dynamic conditions like a sudden change in the applied load, a sudden change in wind speed, and under stochastic wind speed variations as well. The system accuracy in emulating the torque-speed characteristics of the target turbine is also verified.

By extending HIL testing technique to this application, the paper ensures HIL effectiveness in many similar design situation in terms of time and cost. Based on the hardware-in-loop testing results, the proposed DTC-based WTE with its fast torque response was proven to successfully emulate the instantaneous aerodynamics of the wind turbines.

ACKNOWLEDGMENT

The authors are really indebted for Electronics Research Institute for providing all the facilities and resources required to carry out this research.

APPENDIX. I : SCIM PARAMETERS

Rated power	1500 W	Stator leakage inductance	0.016 H/phase
Rated frequency	50 Hz	Rotor leakage inductance	0.0155H/phase
No of pair poles	2	Mutual inductance	0.23 H
Rotor phase resistance	2.553 Ω	Full load input current	4.145 A
Friction coefficient	0.008 N.m.s^2	Moment of inertia	0.15 N.m.s

REFERENCES

1. F. Huerta, R. Tello and M. Prodanovic, "Real-Time Power-Hardware-in-the-Loop Implementation of Variable-Speed Wind Turbines," in *IEEE Transactions on Industrial Electronics*, vol. 64, no. 3, pp. 1893-1904, March 2017.
2. D. Xiang, and T. Wang, "On-Site LVRT Testing Method for Full-Power Converter Wind Turbines," in *IEEE Transactions on Sustainable Energy*, vol. 8, no. 1, pp. 395-403, 2017.
3. L. Gan, M. Mueller, "Modeling and Characterization of Downwind Tower Shadow Effects using a Wind Turbine Emulator," in *IEEE Transactions on Industrial Electronics*, vol. PP, no.99, pp.1-8, 2017.
4. H. Liu, F. Locment and M. Sechilariu, "Experimental Analysis of Impact of Maximum Power Point Tracking Methods on Energy Efficiency for Small-Scale Wind Energy Conversion System," in *IET Renewable Power Generation*, vol. 11, no. 2, pp. 389-397, 2 8 2017.
5. S. Mozayan, M. Saad, H. Vahedi, H. F.chette and M. Soltani, "Sliding Mode Control of PMSG Wind Turbine Based on Enhanced Exponential Reaching Law," in *IEEE Transactions on Industrial Electronics*, vol. 63, no. 10, pp. 6148-6159, Oct. 2016.
6. M. E. Abdallah, O. M. Arafa, "Design and Control of One kilowatt DC Motor-based Wind Turbine Emulator", *International Journal of Engineering Research*, vol. 5, no. 3, pp. 185- 189, March 2016.
7. R. Ovando, J. Aguayo, M. Cotorogea, "Emulation of a Low Power Wind Turbine with a DC motor in Matlab/Simulink," *PESC'07*,

Orlando, FL, June 2007, pp. 859 – 864.
8. S. Kouadria, S. Belfedhal, E. Berkouk, Y. Meslem, “Development of Real Time Wind Turbine Emulator Based on DC Motor Controlled by PI Regulator,” *8th International Conference (EVER)*, Monte Carlo, March 2013, pp. 1 – 5.
9. S. Kouadria, Y. Meslem, E. Berkouk, “Development of Real Time Wind Turbine Emulator based on DC Motor Controlled by Hysteresis Regulator,” *International Renewable and Sustainable Energy Conference (IRSEC)*, Ouarzazate, March 2013, pp. 246 – 250.
10. W. Hu, Y. Wang, X. Song, Z. Wang, “Development of Wind Turbine Simulator for Wind Energy Conversion Systems Based on Permanent Magnet Synchronous Motor,” *International Conference on Electrical Machines and Systems*, Wuhan, Oct. 2008, pp. 2322 – 2326.
11. L. Yang, S. Yan, Z. Chen, W. Liu, “A Novel Wind Turbine Simulator for Wind Energy Conversion Systems Using aPermanent Magnet Synchronous Motor,” *International Conference on Electrical Machines and Systems (ICEMS)*, Busan, 2013, pp. 2156 – 2158.
12. K. Tan, "Squirrel-Cage Induction Generator System Using Wavelet Petri Fuzzy Neural Network Control for Wind Power Applications," in *IEEE Transactions on Power Electronics*, vol. 31, no. 7, pp. 5242-5254, July 2016.
13. H. Voltolini, M. Granza, J. Ivanqui, R. Carlson, “Modeling and Simulation of the Wind Turbine Emulator using Induction Motor Driven by Torque Control Inverter,” *10th IEEE/IAS International Conference on Industry Applications (INDUSCON)*, Fortaleza, Nov. 2012, pp. 1 – 6.
14. A. Abo-Khalil, “A New Wind Turbine Simulator Using a Squirrel-Cage Motor for Wind Power Generation Systems,” *IEEE Ninth International Conference on Power Electronics and Drive Systems (PEDS)*, Singapore, Dec. 2011, pp. 750 – 755.
15. Z. Zhang, R. Tang, B. Bai and D. Xie, "Novel Direct Torque Control Based on Space Vector Modulation With Adaptive Stator Flux Observer for Induction Motors," in *IEEE Transactions on Magnetics*, vol. 46, no. 8, pp. 3133-3136, Aug. 2010.
16. M. Depenbrok, “Direct self-control (DSC) of Inverter-Fed Induction Machine”, *IEEE Trans. Power Electron*., no. 3, pp. 420–429, 1988.
17. M. Depenbrock and A. Steimel, “High Power Traction Drives and Convertors”, *Proc. Elect. Drives Symp*.’90, pp. 1–9, 1990.
18. M. Nikzad, B. Asaei; S. Ahmadi, "Discrete Duty-Cycle-Control Method for Direct Torque Control of Induction Motor Drives with Model Predictive Solution," in *IEEE Transactions on Power Electronics*, vol. PP, no.99, pp.1-10, Mar. 2017.
19. T. Noguchi and I. Takahashi, “Quick Torque Response Control of an Induction Motor Based on a New Concept”, *IEEJ Tech. Meeting Rotating Mach*. RM84-76, pp. 61–70, 1984.
20. I. Takahashi, T. Noguchi, A New Quick-Response and High-Efficiency Control Strategy of an Induction Motor. *IEEE Transactions on Industry Applications*, vol. IA-22, no. 5, pp. 820–827, Sept./Oct. 1986.
21. I. Takahashi and Y. Ohmori, “High-Performance Direct Torque Control of an Induction Motor”, *IEEE Trans. Ind. Applicat.* vol. 25, pp. 257–264, 1989.
22. J. Pandit, M. Aware, R. Nemade and E. Levi, "Direct Torque Control Scheme for a Six-Phase Induction Motor With Reduced Torque Ripple," in *IEEE Transactions on Power Electronics*, vol. 32, no. 9, pp. 7118-7129, Sept. 2017.
23. C. Lascu, S. Jafarzadeh, M. Fadali and F. Blaabjerg, "Direct Torque Control With Feedback Linearization for Induction Motor Drives," in *IEEE Transactions on Power Electronics*, vol. 32, no. 3, pp. 2072-2080, March 2017.
24. I. Alsofyani and N. Idris, "Simple Flux Regulation for Improving State Estimation at Very Low and Zero Speed of a Speed Sensorless Direct Torque Control of an Induction Motor," in *IEEE Transactions on Power Electronics*, vol. 31, no. 4, pp. 3027-3035, April 2016.
25. J. Pandit, M. Aware, R. Nemade and E. Levi, "Direct Torque Control Scheme for a Six-Phase Induction Motor With Reduced Torque Ripple," in *IEEE Transactions on Power Electronics*, vol. 32, no. 9, pp. 7118-7129, Sept. 2017.
26. P. Tiitinen, P. Pohjalainen, J. Lalu, The Next Generation Motor Control Method: Direct Torque Control (DTC). *EPE Journal*, vol. 5, no. 1, pp. 14–18, Mar. 1995.
27. J. Nash, “Direct Torque Control, Induction Motor Vector Control Without an Encoder. *IEEE Transactions on Industry Applications*, vol. 33, no. 2, pp. 333–341, Mar./Apr. 1997.
28. D. Casadei, G. Serra, A. Tani, "Performance Analysis of a DTC Control Scheme for Induction Motor in the Low Speed Range. Proc. *EPE '97*, pp. 3.700–3.704, Trondheim, Norway, Sept. 1997.
29. D. Casadei, G. Serra, A. Tani, Steady-State and Transient Performance Evaluation of a DTC Scheme in the Low Speed Range. *IEEE Transactions on Power Electronics*, vol. 16, no. 6, pp. 846–851, Nov. 2001.
30. D. Krušelj, M. Bilit, B. Furcic, V. Siladi, M. Vuferic, "Direct Torque Control of Induction Motor with Stator Flux Correction", AUTOMATIKA 44(2003) 1-2. 4146.
31. W. Li, D. Xu, W. Zhang, H. Ma., “Research in Wind Turbine Emulation Based on DC Motor,” in *2nd IEEE conference industrial Electronics and Applications*, 2007, pp. 2589-2593.
32. T. Thiringer and J. Linders, “Control by Variable Rotor Speed of a Fixed Pitch Wind Turbine Operating in a Wide Speed Range,” *IEEE trans. energy conv*., vol. 8, pp. 520–526, Sept. 1993.
33. J. Kooning, B. Meersman, T. Vandoorn, L. Vandevelde, “Evaluation of the Maximum Power Point Tracking performance in small wind turbines,” *IEEE Power and Energy Society General Meeting*, San Diego, CA, pp. 1 – 8.
34. M. Żelechowski,"Space Vector Modulated–Direct Torque Controlled (DTC–SVM) Inverter–Fed Induction Motor Drive", Ph.D. Thesis, Warsaw University of Technology, 2005.
35. K. Chouhan and G. Buch, "Improved Direct Torque Control of Induction Motor," *2015 International Conference on Electrical, Electronics, Signals, Communication and Optimization (EESCO)*, Visakhapatnam, pp. 1-5, 2015.
36. F. Bianchi, H. Battista, R. Mantz, and O. Bianchi, Wind Turbine Control Systems: Principles, Modelling and Gain Scheduling Design. London: Springer London, 2006.
37. C. Nichita, D. Luca, B. Dakyo and E. Ceanga, "Large Band Simulation of the Wind Speed for Real Time Wind Turbine Simulators", *IEEE Transactions on Energy Conversion*, vol. 17, no. 4, pp. 523-529, 2002.
38. I. Hoven, "Power Spectrum of Horizontal Wind Speed in the Frequency Range from 0.0007 To 900 Cycles per Hour", *Journal of Meteorology*, vol. 14, no. 2, pp. 160-164, 1957.
39. E. Welfonder, R. Neifer and M. Spanner, "Development and Experimental Identification of Dynamic Models for Wind Turbines", *Control Engineering Practice*, vol. 5, no. 1, pp. 63-73, 1997.